The Simulation and Design of Integrated Inductors

N.R. Belk[1]	M.R.Frei[2]	M. Tsai[2]	A.J. Becker[2]	K.L. Tokuda[2]
Room 4c-422	Room 2d-230	Room 1c-433a	Room 1c-433b	Room 1a-119
732-332-6705	908-582-2514	908-582-5797	908-582-3985	908-582-6571
nrbelk@Lucent.com	frei@Lucent.com	mingju@Lucent.com	bec@Lucent.com	tokuda@Lucent.com

[1] Bell Laboratories, Lucent Technologies, 101 Crawfords Corner Road, Holmdel NJ 07733

[2] Bell Laboratories, Lucent Technologies, 600 Mountain Avenue, Murray Hill, NJ 07974

ABSTRACT

At present there are two common types of integrated circuit inductor simulation tools. The first type is based on the Greenhouse methods[1], and obtains a solution in a fraction of a second; however, because it does not use solutions of the inductor charge and current distributions, it has limited accuracy. The second type, method of moments (MoM) solvers, determines the charge and current variations by decomposing the inductor into thousands of sub elements and solving a matrix. However, this process takes between minutes and hours to obtain a reasonably accurate solution. In this paper, we present a series of algorithms for solving inductors, of radius small compared to the wave length of the electrical signal, that equal or exceed the accuracy of MoM solvers, but obtain those solutions in roughly 1 second.

1. INTRODUCTION

Inductors are commonly used for impedance matching, emitter degeneration and on chip resonant circuits. It is now possible to fabricate "high-Q" inductors on standard IC processes. Designers can use inductors with values of 0.1 to 20nH with Q's of 1 to 15, and with self-resonant frequencies of 1 to 40GHz. Assuming a 10% inter element spacing, a library spanning this range of components would need to include ~50,000 elements. Further, since an inductor is described by many physical characteristics a typical process will support many thousands of reasonable inductor designs making it quite difficult to find an inductor possessing the appropriate characteristics.

The above difficulties are best addressed through fast accurate algorithms for inductor simulation.

We report the algorithms that we have developed for the accurate and rapid modeling of thick or stacked metal inductors on substrates with widely varying conductivities. Because the conductive IC substrates interact with the electromagnetic fields generated by currents in an integrated circuit, an accurate electrodynamic model of the substrate interactions is required to describe the electrical characteristics of inductors. To obtain this, we solve for an electrodynamic vector potential Green's function from which we subtract a zero-frequency static Green's function. The frequency dependent *difference field* Green's function which remains is stored in an array. To determine the characteristics of the inductor, the *difference field* solution is superimposed onto the solution from the static Green's function. Because this *difference field* has a weak spacial dependence it can be accurately incorporated with few calculations.

Further, because the long range frequency dependent component of the scalar potential can be strongly suppressed by substrate grounding, we design our inductors with ample substrate grounding and present a largely static technique for determining the metalization charge distribution. Finally, since the dissipation of eddy currents in inductor metals, and the fringing capacitance of those metals are strongly effected by both the horizontal and the vertical structure of the inductor, we present a technique through which we decompose the inductor into repeated sub units, solve for the field dependent 3 dimensional charge and current distributions on those sub units, and then determine the electrical characteristics of the inductor from those of the sub units. Through these techniques we are able to predict the characteristics of a typical multi-layer inductor to within a few percent in about 1 second.

2. SUBSTRATE INTERACTIONS

In order to determine the effect of substrate coupling on the electrical properties of the inductor, it is necessary to construct a vector potential Green's function for a point current in the vicinity of the substrate. In what follows, the solution for the characteristics of the electric field generated by a point current source located in the metal stack of an IC wafer is described. That field is separated into two components: 1) the field from a static or time invariant point current without substrate interactions, and 2) effects of the substrate on those fields.

The potential Φ describing the radiation arising from a point source of frequency f at $r=0$ is given as the solution to the inhomogeneous Helmholz wave equation:

$$\left[\nabla^2 + \frac{(2\pi f)^2}{c^2}\right]\Phi(r,f) = \delta(r),$$

(1) where c is the speed of light in the media. The electric field generated by this current element is:

$$E(r,f) = 2\pi i f \mu_0 \left(\bar{I} + \frac{\nabla\nabla}{k^2}\right)\Phi, \qquad (2)$$

where $k=2\pi f/c$, $\bar{I}$ is the identity matrix and r is the vector between the source current and the observation point. The derivatives on the right of Eq.2 describe the field from the scalar potential while $\bar{I}$ determines the component arising from the vector potential. For a metal segment 100µm in length, the component of the field from the scalar potential $[O(1/r^3)]$ will be many orders of magnitude larger than that from the vector potential $[O(1/r)]$ and will complicate the accurate evaluation

of the component arising from the vector potential. In addition, because of the small size of the segment, the component of the field arising from the scalar potential will result in a displacement current parallel to that segment which is orders of magnitude smaller than the current through that segment. Further, because the time dependent magnetic field arising from this displacement current does not couple strongly to the metal segment, the fields arising from the displacement current are not important for segments of dimensions < *c/(10f)* ~ 1 cm. For these reasons, in Eq.2 we retain only the component of the electric field arising from the vector potential and address the scalar potential interactions separarely.

2.1 Inductive Substrate Coupling

In inhomogeneous planar media, we use Somerfeld's[2] identity for our determination of the potential $\Phi(\boldsymbol{r}, z)$:

$$\Phi = i\int_0^\infty dk_{\boldsymbol{r}} \frac{k_{\boldsymbol{r}}}{k_z} J_0(k_{\boldsymbol{r}}\boldsymbol{r})\left[e^{ik|z-z'|} + A_+ e^{-ik_z z} + A_- e^{ik_z z}\right]. \quad (3)$$

where z' is the height of the source, A_+ and A_- are the complex amplitude of the waves reflected from above and below the metalizations respectively. Equation 3 the potential into an integral over evanescent and traveling waves$\left(e^{ik_z|z|}\right)$ in the $\hat{z}$ direction and cylindrical waves$\left[J_0(k_r\boldsymbol{r})\right]$in the $\hat{\boldsymbol{r}}$ direction with $k^2 = k_{\boldsymbol{r}}^2 + k_z^2$.

For IC substrates, the wave propagation in the $\hat{z}$ direction is determined by the *Fresnel* transverse electric reflection and transmission coefficients[3] at each dielectric interface[4]. With the determination of A_+ and A_- [5], we determine the potentials arising from the point current in the vicinity of the substrate. The substitution of Eq.3 into Eq.2 determines the in plane electric fields $E(\boldsymbol{r}, z)$ at all places in the metalization stack arising from current dipole $\hat{x}I(\boldsymbol{r}', z')d\ell$ anywhere in the metal stack and which is generally expressed in the following form:

$$E(\boldsymbol{r}, z) = \hat{x}I(\boldsymbol{r}', z')d\ell \frac{if}{\mathbf{e}_0 c^2}\int_0^\infty k_{\boldsymbol{r}} G \cdot J(k_{\boldsymbol{r}}\boldsymbol{r})dk_{\boldsymbol{r}}.$$

(4). The form for the electric field in Eq.4 is inconvenient because the integral converges slowly and E diverges as $1/\boldsymbol{r}$ for small $\boldsymbol{r}$, making the evaluation of the self induced fields difficult. The divergence can be removed by observing that:

$$\int_0^\infty J_0(k_{\boldsymbol{r}}\boldsymbol{r})dk_{\boldsymbol{r}} = 1/\boldsymbol{r}. \quad (5)$$

As a result, the field at $(\boldsymbol{r}, z)$ arising from a point current source $I(\boldsymbol{r}', z')$ can be written as:

$$\bar{E}(\boldsymbol{r}, z) = \frac{if\, Id\bar{\ell}}{2\boldsymbol{e}_0 c^2}\left[\begin{aligned}&\int_0^\infty \left(k_r G(z, z') - \frac{1}{2}\right) J_0(k_r|\boldsymbol{r} - \boldsymbol{r}'|)dk_r \\ &+ \frac{1}{2|\boldsymbol{r} - \boldsymbol{r}'|}\end{aligned}\right] \quad (6)$$

The second term in the square brackets on the right of Eq.6 is Neuman's Equation for the electric fields generated by current carrying elements in free space at zero frequency. Induced substrate currents dominate the integral on the right of Eq.6. Because the skin depth in the IC substrate is >100µm, the fields arising from the substrate coupling are a slowly varying function of $\boldsymbol{r}$ and can be evaluated at intervals of $\boldsymbol{r}$ ~5µm and at frequency intervals of ~ 0.5 GHz. We store the frequency and position dependent values in the array $\Xi_{f,\boldsymbol{r}}$ that we use as a look up table.

2.2 Capacitive Substrate Coupling

For the scalar potential we use static images to describe the fields from metalization charges and also to describe the dominant component of the scalar potential substrate coupling generated by the induced surface charge that resides at the boundary between the conductive substrate and the insulating oxides. This initial approximation is accurate as long as the capacitive impedance of the oxides is much greater than the resistive impedance of the substrate underlying the inductor. We insure that this condition is met by automatically generating a poly-silicon and metal substrate grounding structure with each inductor design. This has the added advantage that it greatly reduces the capacitive part of the inductor to circuit cross talk. Once the metalization charge distributions are determined statically we back calculate the loss they would generate in the substrate grounding structure.

3. METALIZATION SOLUTION

3.1 Representative Sub Units

It is possible to completely solve this problem with Eq.6 and the static approximation for the shielded scalar potential discussed above. However, we can substantially reduce simulation times by taking advantage of the slowly varying nature of the currents and potentials generated by the signals propagating through the length of the structure. In what follows we discuss two simulation algorithms. The first for strongly coupled symmetrical structures like the inductor body, and the second for lower symmetry structures such as the inductor leads. We solve for the characteristics of the overall inductor by selecting representative sub units from it, determining the characteristics of those sub units, then determining the characteristics of the inductor from a suitable combination of the sub unit characteristics.

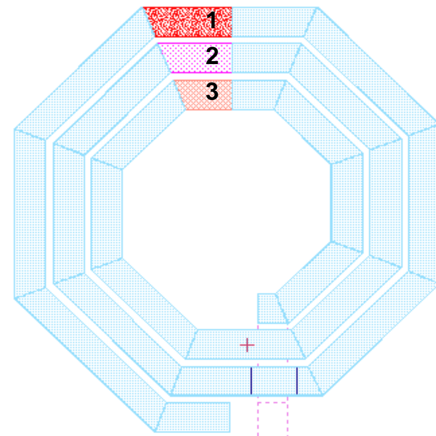

Fig.1 shows an optimized three turn integrated inductor with three numbered representative sub units selected from it.

Since the physical dimensions of the sub units are small compared to the wavelengths of the electrical signals, they can have current and charge distributions prescribed to them independently. Further, since the sub unit characteristics can be

made field and size dependent, this technique is robust against large variations in inductor design.

The sub units are broken down into an array of short and long metal elements or paths carrying a current or charge distribution that must be determined. In both the solution for the characteristic of the sub units and the solution of the overall structure, we begin with a static solution on the metals then superimpose the substrate interactions (Eq.6) on that solution. In what follows we discuss the solution of the series impedances and parallel admittances of the IC inductor through the determination of the 3 dimensional charge and current distributions on representative sub units and then building the solution for the inductor from the properties of those distributions.

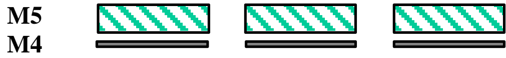

Fig.2 Shows the cross section of the three sub units selected from the body of the inductor in Fig.1. In the meshing of this structure we use 3 vertically stacked layers of sub elements for the thick metal (M5) and 1 layer for the thin metal (M4).

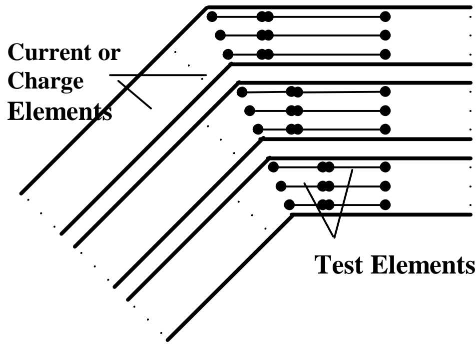

Fig.3 shows the decomposition of the three sub units into sub elements. Although the elements are depicted in two dimensions in the material presented below, it is assumed that they are arrayed three dimensionally.

As shown, on or near each of the current or charge carrying elements is a "test element" which spans the region between the dots on the current or charge carrying element. In this work, the test elements are smaller than the charge or current carrying elements but they fully span the sub unit.

The field or potential on each of the test elements arising from the current or charge on all of the longer elements is determined by the sum of two components. The first, the self induced field of a charge or current element of radius ρ whose endpoints are offset from those of the test element by the distances $x_{a,b} = x_{i,a} - x_{j,b}$ in the direction parallel to their lengths is determined by:

$$ms_{i,i} = \frac{\mu_0}{2\pi} \sum_{a=-1}^{1} \sum_{b=-1}^{1} (-1)^{a+b} \cdot \left[\frac{\left(\rho^2 + x_{a,b}{}^2\right)^{3/2} - \left|x_{a,b}\right|^3}{3\rho^2} + \frac{\left|x_{a,b}\right|}{2} \cdot \log\left(\frac{2 \cdot x_{a,b}}{\rho}\right) \right]. \qquad (7)$$

where the form for the scalar potential ϕs is the same except that the constant $\mu_0/2\pi$ is replaced by $1/2\pi\varepsilon$. The second component, arising from the coupling of the test elements to adjacent lines of current or charge or the charge images that are separated from the test element can be determined by[6]:

$$m_{i,j} = \frac{1}{4\pi\varepsilon_0 c^2} \int_0^{l_i} \int_0^{l_j} \frac{1}{\left|\bar{r}_i - \bar{r}_j\right|} \overline{dl}_i \cdot \overline{dl}_j \qquad (8)$$

$$\phi_{i,j} = \frac{1}{4\pi\varepsilon} \int_0^{l_i} \int_0^{l_j} \frac{1}{\left|\bar{r}_i - \bar{r}_j\right|} - \frac{1}{\left|\bar{r}_i - \bar{r}_j - 2z\hat{z}\right|} dl_i dl_j \qquad (9)$$

where $\bar{r}_j$ and $\bar{r}_i$ are the locations of the observation and source points respectively and $2z\hat{z}$ is the height of the source above the image. Although Eq.8 and 9 is useful, in our simulations we use closed form expressions for the interactions between straight elements derived from Eq.8 and 9 which we will not describe in detail here[1,7].

3.2 Sub Unit Impedance Determination

The zero frequency self resistance of the test elements is:

$rs_i = Rm\, ln_i / w_i th_i$,

(10) where Rm is the metal resistivity, w_i is the width, th_i is the thickness, and ln_i is length of the test element.

The component of the electric field arising from the substrate interactions can be determined through the following equation:

$$z_{i,j} = \sum_{0}^{\frac{ln_j}{\Delta\ell_j}} \sum_{0}^{\frac{ln_i}{\Delta\ell_i}} \Xi_{f,\rho} \overline{\Delta\ell_i} \cdot \overline{\Delta\ell_j}, \qquad (11)$$

where the $\Xi_{f,\rho}$ are coefficients from the substrate coupling matrix. The vectors $\overline{\Delta\ell_i}$ and $\overline{\Delta\ell_j}$ are the summation intervals, ρ is the separation between the centers of the summation intervals, and the summations are over every element in the sub unit. Because the microwave penetration depth into silicon substrate is large compared to inductor metal widths, the spatial variation of $\Xi_{f,\rho}$ is weak and does not significantly affect the details of the sub unit current distributions in our inductors.

The series impedances described above are combined in the form:

$$\delta V_i = \left(2\pi f ms_{i,i} + rs_i + z_{i,i}\right) I_i + 2\pi f \sum_{\neq j} I_j \left(m_{i,j} + z_{i,j}\right), \qquad (12)$$

where δV_i is the voltage across the ith metal test element arising from the currents in each of the jth segments and are taken to be the same for all parallel test elements. If all three sub units are solved simultaneously, Eq.12 will run over all current and charge elements in the three sub units. Since it is often necessary to find the physical characteristic of the sub units in the external electric field arising from the currents in other sub units, the effect of external fields can be added to the left of Eq.12 through terms of the form:

$$E(x_0) + \frac{\partial E(x_0)}{\partial x} \cdot (x - x_0) + \frac{\partial^2 E(x_0)}{\partial x^2} \cdot \left[\frac{3}{2}(x - x_0)^2 - \frac{1}{2}\right] + \ldots \qquad (13)$$

where x is taken to be along the line which intersects the ends of the parallel test segments, x_0 is at the center of the sub unit, the magnitude of the external field E and its derivatives are adjustable parameters and the lengths are normalized such that x

is between –1 and -1 so that the terms are orthogonal. Because the inductor body in Fig.1 is strongly symmetrical, and because the wavelengths of the electrical signals (≥ 3 cm) are much greater than an inductor diameter, the external E-field on the sub unit (Eq.13) can be approximated as arising from uniform currents in large sections the inductor. As a result, in the inductor in Fig.1 each turn, including its sub unit, can be excited with a current independently, the three sub units can be solved for each excitation, and the sub unit current distribution and electrical properties can be determined as a function of its self and adjacent turn currents.

For structures lacking the symmetry of the inductor in Fig.1, it is often desirable to solve Eq.12 and 13 independently for the important terms in the electric field expansion (Eq.13) so that the field dependence of the sub unit current distribution and therefore its electrical properties can be determined.

Because the sub units are small compared to the wavelength of the electrical signal, the currents in the parallel filaments is roughly constant so for sub units being excited:

$$\sum I_j = 1 \qquad (14)$$

for sub units which are not being excited, the constraint is:

$$\sum I_j = 0 \qquad (15)$$

The simultaneous solution of Eq.12 and 13 with the constraints in Eq.14 and or 15 allow us to obtain the field dependent current distribution of the sub unit.

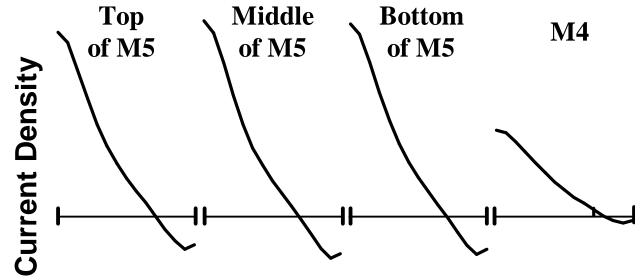

Fig.4 Shows the current distribution in each of the four vertical mesh layers in the inside turn sub unit (#3) of the inductor in Fig.1 and Fig.2 at 2GHz with excitation currents in all three turns. The figure is drawn such that the inside edge of each layer of the sub unit is to the left and the horizontal sub unit layer is drawn at a height corresponding to *I=0*. As seen in this figure the circulating eddy currents in this metal are large enough that the current reverses direction near the right edge. These eddies are due to the currents in the outer turns of the inductor.

In order to determine the electrical characteristics of the sub unit, we use the current distribution on the sub unit and the voltage difference on the left of Eq.12.

The complex in field sub unit impedance is determined by the sub unit voltage differences $\mathbf{d}_i$ divided by the sub unit current:

$$Z_{i,j} = \mathbf{d}_i / I_j$$

(16)

Equation 16 describes the system included in Eq.12 and 13.

Variations in the sub unit electrical properties arising from variations in sub unit length can be determined by decomposing the sub unit of perturbed length into the sum of the original sub unit plus a short extension to the sub unit. The self and mutual characteristics of the sub unit extension can be determined through substitution of the previously determined sub unit current distribution into Eq.7 and 8 to solve the self and mutual interactions between the current elements and the sub unit extension.

3.3 Mutual Sub Unit Inductance

The Mutual interactions between a sub unit extension and another sub unit or between two sub units *A* and *B* can be determined through:

$$M_{A,B} = \sum_i \sum_j m_{i,j} I_{A,i} \cdot I_{B,j} \qquad (17)$$

where the $I_{A,i}$ and the $I_{B,j}$ are the currents on the ith and j^{th} test elements on the Ath and B^{th} sub units respectively.

A more efficient manner for the determining and expressing the mutual interactions between sub units is through multipole decomposition. The current distributions on the sub units are decomposed into mathematically orthogonal functions. These current distribution functions generate electric fields whose spatial dependence is stored in look up tables and the electric fields can then be used to determine the couplings of the adjacent sub units. Convenient current distribution functions are: $f_n = 1, x, 3x^2/2 - 1/2, \ldots$. These functions are chosen because as *n* increase the field generated by these distributions falls of more rapidly with distance and the long range couplings become less important. The magnitude of the component a_n of each f_n in a sub unit current distribution is:

$$a_n = \frac{2n+1}{N} \sum_{i=0}^{N-1} f_n\left(\frac{2i-N+1}{N-1}\right) \cdot I_i \qquad (18)$$

The electric field generated by a_n is given by:

$$E_n(2\mathbf{r}/w, \mathbf{q}) = \frac{if\mathbf{m}_0 N}{2w} \int_{-1}^{1} \frac{a_n f_n dx}{\left(\mathbf{r}^2 + 2\mathbf{r}x\cos\mathbf{q} + x^2\right)^{1/2}} \qquad (19)$$

where *w* is the width of the sub unit $\mathbf{r}$ is the distance to the center of the distribution being represented and $\mathbf{q}$ is the angle between the current flow and line between the source and observation points. For wide metals on highly conductive substrates the results of Eq.19 may be combined with $z_{i,j}$ (Eq.11). Because $M_{i,j} \propto \int_0^{Ln_j} \int_0^{Ln_i} dl_i dl_j E(\mathbf{r}, \mathbf{q}) / I_i I_j$ for line of current, the E-fields from the sub units also determine the mutual inductances between sub units. This mutual inductance can be calculated by integrating the E_n over the sub unit current distributions, however, it is more efficient to use the a_n determined above in conjunction with the look up tables for E_n to calculate $M_{i,j}$.

To determine the overall system of series impedances it is necessary to first assemble the system from the solved sub units, determine the coupling between the sub units, and tabulate these properties with their self impedances. The component of the induced fields between sub units arising from the substrate interactions can be determined through Eq.11. where the summations are over every sub unit of length Ln_i in the system. The series impedances described in Eqs.16 through 19 are then combined in the form:

$$V_i - V_{i-1} = (z_{i,i} + Z_{i,i}) I_i + 2\mathbf{p} i f \sum_{j \neq i} I_j \left(M_{i,j} + z_{i,j} + Z_{i,j}\right), \qquad (20)$$

where $V_i - V_{i-1}$ is the voltage across the ith sub unit arising

from the currents in each of the jth sub units and the $M_{i,j}$,are the appropriate weighted sums over the sub unit a_n and E_n discussed above. This determination of $M_{i,j}$ can be improved if the a_n and E_n are solved self consistently with Eq.20. However, we will not address this in the present work.

3.4 Sub Unit Admittance Determination

To determine the complex admittance matrix for the inductor, the potentials described in Eqs.7 and 9 are combined in the form:

$$\boldsymbol{f}_j = \boldsymbol{f}s_{j,j}q_j + \sum\nolimits_{i\neq j} \boldsymbol{f}_{i,j}q_j \, . \tag{21}$$

The $\boldsymbol{f}_j$ are generally the same for all test elements. If all three sub units are solved simultaneously, Eq.21 will run over all charge elements in the three sub units.

To find the physical characteristic of the sub units in the external potential arising from the charge on other sub units, a potential can be added to the left of Eq.21 through terms of the form:

$$\Phi(x_0) + \frac{\partial\Phi(x_0)}{\partial x}\cdot(x-x_0) + \frac{\partial^2\Phi(x_0)}{\partial x^2}\cdot\left[\frac{3}{2}(x-x_0)^2 - \frac{1}{2}\right] + \ldots \tag{22}$$

where x is taken to be along the line which intersects the end of each of the parallel test segments, x_0 is midway through the sub unit, we adjust the magnitude of the potential Φ and its derivatives and the lengths are normalized such that x is between -1 and 1. Unlike the metalization currents, there can be variation in magnitude of the charge along the length of the metalization so additional terms can be added to Eq.22 to account for these variations, however these variations tend to be limited by the screening effects of the substrate.

In structures such as the inductor in Fig.1 The sub unit in each turn can be excited with a voltage independently, the three sub units can be solved for each excitation, and the sub unit charge distribution and electrical properties can then be determined as a function of their self and adjacent turn voltages.

For structures lacking the symmetry of the inductor in Fig.2, it is often desirable to solve Eq.21 and 22 independently for each significant term in the potential expansion so that the dependence of the sub unit charge distribution and its electrical properties on the potential or its derivatives can be quantified. As a result, in the solution of the overall system, the effects of the field dependence of a sub unit charge distribution is accurately represented.

Because the sub units are small compared to the wavelength of the electrical signal, the voltages of the elements in and connected to the excited sub units are:

$$\boldsymbol{f}_i = 1$$

(23) for sub units which are not being excited, the constraint is:

$$\boldsymbol{f}_i = 0$$

(24) As describe above, the simultaneous solution of Eq.21 through Eq.24 allows us to obtain the field dependent charge distribution of the sub unit.

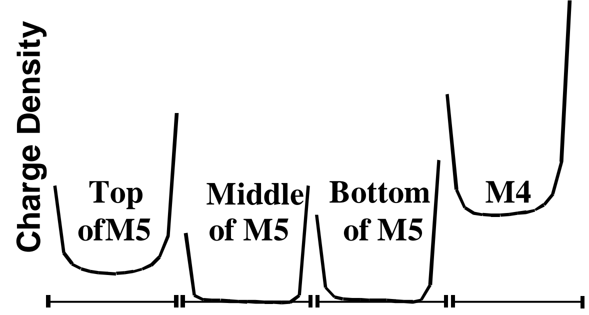

Figure 5 shows the charge distribution in each of the four vertical layers in sub unit #3 of the inductor in Fig.1 and Fig.2 with excitation voltage on only the inside turn. The figure is drawn such that the inside edge of each layer of the sub unit is to the left on the figure and the sub unit layer is drawn at a height corresponding to *q=0.* As seem in this figure most of the charge resides on the upper and lower metal surfaces. All of the distributions are slightly higher on the right side due to the presence of the outer inductor turns.

In order to determine the characteristics of the sub unit, we use the charge distribution on the sub unit as well as the sub unit voltages $\boldsymbol{f}_i$ on the left of Eq.21. The sub unit voltage divided by the total sub unit charge *qtot* determines the complex in field sub unit admittance.

$$Yp_{i,j} = i2\boldsymbol{p}fqtot_i / \boldsymbol{f}_j \tag{25}$$

Variations of the sub unit self and mutual electrical properties which arise from variations in sub unit length can be determined by decomposing the sub unit of perturbed length into the sum of the original sub unit plus a short physical extension to the sub unit. The self and mutual characteristics of the sub unit extension can be determined through the previously determined sub unit charge distribution and Eq.7 to Eq.9 to describe the self and mutual interactions between charge elements and the sub unit extension.

3.5 Mutual Sub Unit Admittance

The Mutual interactions between two sub units *A* and *B* can be determined through:

$$C_{A,B} = \sum_i \sum_j \boldsymbol{f}_{i,j}\, q_{A,i} q_{B,j} / V^2 \tag{26}$$

where the $q_{A,i}$ and the $q_{B,j}$ are the charges on the Ath and B^{th} sub units respectively.

As discussed previously, a more efficient manner for the determining and expressing the mutual interactions between sub units is through a multipole decomposition as in Eq.18 and 19.

The parallel metalization self and mutual admittances of the overall system are determined through the suitable combination of the representative sub units to form the larger system and the tabulation of their characteristics and interactions when assembled into the larger system in the following form:

$$I_{j-1} - I_j = V_j Yp_j + 2\boldsymbol{p}if \sum_{i\neq j} (V_j - V_i) C_{i,j} \, . \tag{27}$$

In Eq.23, the $I_{j-1} - I_j$ represent currents that are diverted from the series paths through parallel impedances. In Eq.27 the Yp_j, describing the capacitive and resistive admittances to the grounded substrate are more important than the $C_{i,j}$ which describe inter sub unit capacitances.

The series impedances in Eq.20 are combined with a set of linear equations describing the parallel impedances Eq.27 and the resulting system of equations is solved for the 2-port frequency dependent network impedances.

4. RESULTS

Through these techniques of utilizing an in plane vector potential Green's function to model inductive substrate coupling, strong substrate grounding to screen capacitive interactions, and a 3 dimensional basis function to model the charge and current distributions, we have simulated many thousands of inductors. Based on these simulations we have fabricated hundreds of optimal designs which we have characterized. These fabricated inductors have had from 1 to 10 turns, and metal widths from 1 to 70 microns, with diameters from 45 to 600 microns.

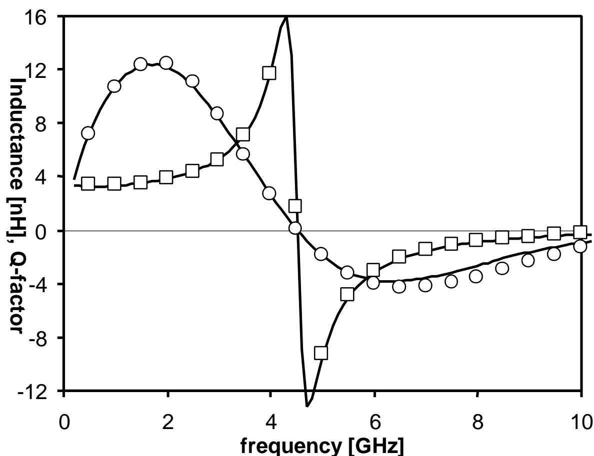

Figure 5 shows the fit of these algorithms to the measured data.

Plotted above are both the measured data (solid lines) and the fit of the model to the effective inductance (□) seem looking into the high Q port of the inductor $\mathrm{Im}\left[(2\pi f y11)^{-1}\right]$. Also plotted are fits of the inductor Q (○) to measured data, where as a definition for Q, we have used $-\mathrm{Im}\left[(y11)^{-1}\right]/\mathrm{Re}\left[(y11)^{-1}\right]$.

The data in Figure 5 were obtained for a 4nH inductor fabricated on a 0.25 micron IC process with a thick low resistance upper level metal. Because of process variations are, we have used experimentally determined values of oxide thickness and the zero frequency metal resistance rather than the nominal values.

As shown in this figure, the model accurately describes the characteristics of this inductor over a frequency range that is much greater than the 2GHz design optimum for the inductor. The errors in these fits are well within the process variation and could readily be explained by the variability in substrate conductivity for which we used the nominal value.

These points were obtained at a rate of roughly one simulation per second. This is a thick metalization inductor, for which the skin effect resistivity reduced the inductor Q by almost a factor of 2. A solution with a MoM solver on this inductor with comparable accuracy requires roughly one half hour per point.

5. CONCLUSION

Because integrated circuit components are physically small compared to the wavelengths of the electrical signals which they carry, the potentials and currents are slowly varying. Although a very dense 3D mesh is often required to accurately capture capacitive fringing fields or metalization eddy currents in thick or stacked metal inductors, those current distributions are highly similar in physically similar structures. As a result, the couplings between metalization subunits and the variations in their charge and current distributions arising from those couplings can be accurately incorporated with few calculations.

Based on these characteristics, we have built algorithms which involve the fine 3D meshing and solviing of the charge and current distributions of those representative structures, the applications of those charge and current distributions to similar metailzation structures. The substrate coupling and the interactions between these structures are then efficiently mapped onto the metalization structures. These techniques have allowed us to accurately extract electrical characteristics from IC metalization structures very rapidly.

6. ACKNOWLEDGEMENTS

We thank Kirk Ashby, Shahriar Moinian, and Vance Archer for many helpful discussions.

7. REFERENCES

[1]E. Pettenpaul, et al., IEEE trans.on microwave theory and techniques,36(2):294-304, Feb 1988.

[2]Sommerfeld, A. 1949. Partial Differential Equations in Physics. New York:Acedemic Press.

[3]Born, M. and E. Wolf. 1980 Principles of Optics. New York:Pergamon Press.

[4]Bellman, R., and G. M. Wing. 1975. An Introduction to invariant Imbedding. New York:John Wiley & Sons.

[5]Chew, W.C., 1995 Waves and Fields in Inhomogeneous Media. IEEE Press Piscataway, NJ.

[6]R.L. Remke and G.A. Burdick, Spiral Inductors for Hybrid and MicroWave Applications, in Proc. 24th Electron Components Conf. (Washington, DC) May 1974, pp. 152-161.

[7]U.A. Shivastava, Fast and Accurate Algorithms of Self and Mutual Inductances of Rectangular Conductors, 8th Ann. Int. elect. Packag. Conf., IEPS-8, pp. 488-507, Nov.1988.